

## Coarse-Grained, Implicit Side-Chain Model of Bottlebrush Polymer Melts

Haisu Kang, Tianyuan Pan, and Charles E. Sing\*

Cite This: *Macromolecules* 2024, 57, 8240–8252

Read Online

ACCESS |



Metrics &amp; More



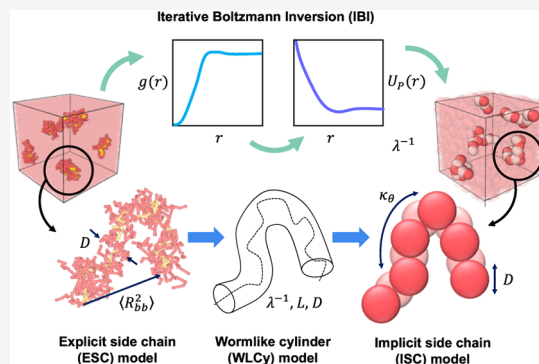
Article Recommendations



Supporting Information

**ABSTRACT:** The unique architecture of bottlebrush polymers gives rise to multiple molecular parameters consisting of the bottlebrush backbone length ( $N_{bb}$ ), side chain length ( $N_{sc}$ ), and grafting density ( $f$ ). These macromolecules can thus be engineered to exhibit a wide range of desired properties, enabling their use in applications ranging from soft elastomers to self-assembled photonic crystals. However, understanding the physical behavior throughout this wide design space is challenging due to the significant computational cost of molecular models. In this work, we designed a coarse-grained model based on the recently developed implicit side-chain (ISC) framework to describe the conformation of bottlebrush polymers in melts. Using single chain in mean-field (SCMF) simulations, we used molecular observables such as the end–end distance  $\langle R_{bb}^2 \rangle$  and radius of gyration  $\langle R_g^2 \rangle$  to parametrize an ISC model with wormlike cylinder model

parameters; effective Kuhn length  $\lambda^{-1}$ , cylinder length  $L$  and width  $D$ . We considered a wide range of bottlebrush architectures, systematically varying the backbone and side-chain lengths ( $N_{bb}$  and  $N_{sc}$ , respectively) and the grafting density  $f$ . We observed that the conformations of bottlebrush polymers follow Gaussian chain conformations at sufficiently long  $N_{bb}$  and are much more flexible than the analogous chains in solution. These bottlebrush polymers exhibit modest stretching, which becomes much more pronounced at high grafting densities ( $f = 5$ ) to accommodate the crowded side chains. Each architecture varying  $N_{bb}$ ,  $N_{sc}$ , and  $f$  could be mapped to a unique set of wormlike cylinder model parameters, so that they can be represented by an ISC model consisting of  $N_{ISC}$  beads of size  $D$  with a bending parameter  $k_\theta$  related with effective Kuhn length  $\lambda^{-1}$ . The effective pairwise interaction potential for this ISC model was determined by using an iterative Boltzmann inversion (IBI) procedure to match the structural features in the ESC model. The resulting interaction potential determined by IBI was consistent with the original architectures, showing similar forms relative to the width  $D$ . However, we observed several trends, such as the emergence of a stronger repulsive potential for longer side chains and higher grafting densities, which we attribute to the increased exclusion of neighboring bottlebrushes due to the higher concentration of grafted side chains. The final ISC model results in a significant reduction of the degrees of freedom needed to model the melt state, and we expect that our melt ISC model for bottlebrush polymers will enable efficient large-scale simulation to relate macroscopic properties to molecular structure.



## 1. INTRODUCTION

Bottlebrush polymers have emerged as a useful molecular architecture for material design. They are characterized by densely grafted side-chains on a linear backbone,<sup>1,2</sup> which leads to a large molecular parameter space including length of backbone ( $N_{bb}$ ), length of side-chains ( $N_{sc}$ ), and the number of grafted side chains ( $f$ ). Side chains and backbones in bottlebrush polymers can be also synthesized with different monomers, introducing another dimension to the design space on top of their architecture parameters.<sup>2–16</sup> This leads to several distinct designs of copolymers such as block copolymers,<sup>2–14</sup> core–shell,<sup>3,5–7,13,15</sup> Janus,<sup>12,16</sup> and random copolymers.<sup>9,14</sup> Their design space provides us the opportunities to explore their properties for a wide range of applications such as photonic and photonic crystals,<sup>17–20</sup> molecular pressure sensors,<sup>21–23</sup> pH-responsive surfaces,<sup>24</sup>

adhesives,<sup>25–27</sup> self-healing materials,<sup>23,28,29</sup> and low-modulus elastomers<sup>30–32</sup> capable of strain hardening and sustaining significant deformation. The utility of these applications arises from several unique consequences of the densely grafted side chains; crowding of the side chains leads to a stiffer molecular contour and thus extended conformations.<sup>1,2,8,33</sup> The stiffening of the backbone also reduces molecular entanglements in bottlebrush melts,<sup>33–35</sup> and aligned ordering has been

Received: May 7, 2024

Revised: July 2, 2024

Accepted: August 1, 2024

Published: August 10, 2024



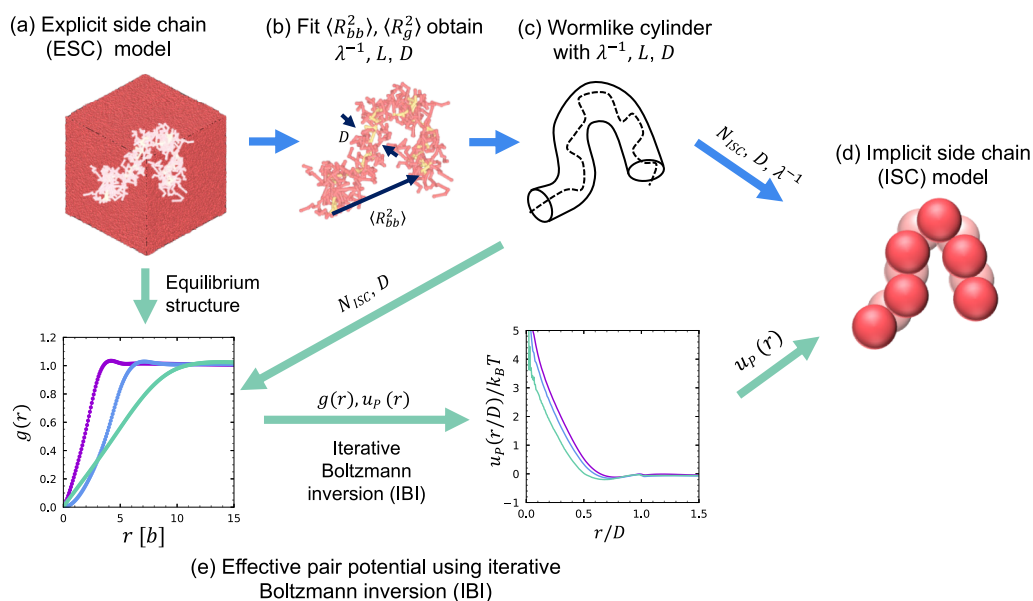


**Figure 1.** Schematic showing the workflow of building ISC model in melts. (a) The fine-grained ESC model is simulated using SCMF simulations. (b) The dimensions of these chains are systematically parametrized by fitting  $\langle R_{bb}^2 \rangle$  and  $\langle R_g^2 \rangle$  to the WLCy model to obtain the fit parameters  $L$ ,  $\lambda^{-1}$ , and  $D$ . (c) This allows us to represent bottlebrush polymers in the melt state as wormlike cylinders, which can then be represented using the ISC model; (d) this model is composed of  $N_{ISC} = (2L - D)/D$  tangent beads with a diameter  $D$  (pink spheres), connected at a distance of  $D/2$  to exhibit a cylinder-like shape, and a bending potential with a bending constant  $k_\theta$  that is related to the Kuhn length  $\lambda^{-1}$ . (e) A pairwise interaction potential  $u_p(r)$  is determined using an IBI method, which improves the pair potential  $u_p(r)$  to match  $g(r)$  from the ISC model system to the corresponding target  $g_{target}(r)$  from the ESC model system.

observed in the liquid state.<sup>36,37</sup> Taking advantage of a large design space and unique properties of bottlebrush polymers for functional and self-assembled materials, however, requires a detailed understanding of how molecular architectural parameters ( $N_{bb}$ ,  $N_{sc}$ ,  $f$ ) affect macroscopic behaviors.

Several different molecular models have been employed to predict how these molecular parameters affect the behavior of bottlebrush polymers in both the melt and solution states.<sup>14,38–49</sup> These efforts include particle-based approaches such as Monte Carlo (MC),<sup>38,50</sup> molecular dynamics (MD),<sup>40,41,51–53</sup> and Brownian dynamics (BD) simulations.<sup>44,45,54,55</sup> Alternatively, field-based models such as self-consistent field theory,<sup>14,56</sup> single-chain in mean-field (SCMF) simulation,<sup>49</sup> theoretically informed coarse-grain simulation,<sup>57</sup> and polymer reference interaction site model theory<sup>42</sup> have also been employed to understand the conformational attributes of bottlebrush polymers. Finally, scaling theories are widely used to extend theoretical knowledge of chain statistics to bottlebrush architectures, offering predictions of scaling exponents.<sup>33,58–60</sup> The primary focus of all these studies revolves around key questions of how to predict bottlebrush conformation and thermodynamics.<sup>61</sup> Despite significant progress in modeling bottlebrush polymers, substantial computational limitations persist, particularly concerning the time scale and length scale over which these macromolecules can be simulated.<sup>45,61</sup> Low-cost single-chain or solution simulations are useful for understanding fundamental properties,<sup>40,45,62,63</sup> but they are limited in their ability to predict macroscale bulk properties that involve the interactions between bottlebrush chains.<sup>64</sup> For multichain bulk simulations, it is challenging to account for the large number of degrees of freedom, because the side-chain behavior plays such an important role in their overall properties<sup>33,46,65</sup> and must be taken into account. These limitations are apparent in particle-

based simulations; cost-effective field-based simulations are a promising alternative but possess fundamental limitations in capturing nonmean-field compositional fluctuations important in these molecules.<sup>14,48,49</sup>

We have recently devised a coarse-graining method to overcome these limitations in modeling bottlebrush polymers in dilute and semidilute solutions.<sup>44,45,54,66,67</sup> Our approach was to first introduce an explicit side-chain (ESC) model. The ESC model is a fine-grained representation of the bottlebrush polymers that includes the grafted side chains and has been parametrized against experimental data on single-chain properties.<sup>47,66</sup> We subsequently demonstrated that these models can be systematically transformed into an implicit side-chain (ISC) representation, which utilizes a wormlike cylinder (WLCy) model to describe the molecular conformation with only four parameters: a Kuhn length ( $\lambda^{-1}$ ), a contour length ( $L$ ), a thickness ( $D$ ), and an excluded volume parameter ( $B$ ).<sup>37,44,45,68,69</sup> With this parametrization, the side-chain degrees of freedom can be coarse-grained; individual bottlebrush chains can be modeled with a simple linear bead–spring chain, where stiffness and bead size are functions of side-chain length and grafting density.<sup>44,45</sup> We demonstrated the efficacy of this model in describing a variety of observables, including the equilibrium size of a single chain, radius of gyration, intrinsic viscosity, hydrodynamic radius, and molecular elasticity under moderate stretching forces or flow.<sup>43,45,55</sup> We further expanded this model to a multichain system and demonstrated the emergence of self-assembled structures in diblock bottlebrush copolymers.<sup>44,54,70</sup> Brush–brush interactions were accounted for using a combination of scaling theory and simulations of a segmental potential of mean force (PMF).<sup>44,54,70</sup> Recently, the ISC framework has been modified to account for semidilute concentrations using the scaling theory that defines how much the pervaded volume

of bottlebrush polymers overlaps by concentration.<sup>67</sup> This ISC model successfully reproduced the concentration-driven structure in printed bottlebrush assemblies.<sup>67</sup> Despite the success of this coarse-graining scheme, it has been exclusively used to study bottlebrush polymers in the solution state.<sup>44,67,70</sup> When solvent interactions are absent and the bottlebrush polymers enter the melt state, their conformations are now significantly more flexible.<sup>33,46,65,71,72</sup> The effect of architecture is now driven by conformational correlations where the total volume of the branches exceeds the pervaded volume expected for random coils.<sup>33,46,65,71–74</sup> This makes it a challenge to describe how architecture affects molecular conformation, as compared to the solution state that is mainly driven by the excluded volume interactions from crowded side chains.<sup>33,45,64,65,75</sup> The prior ISC model estimates the conformation in concentrated solution relative to the dilute condition using the scaling theory,<sup>67</sup> which is unable to predict the true architecture-driven conformation in melts. It is therefore important to develop a new framework for finding an analogous ISC model that can accurately model conformations and structures in the melt state.

In this study, we adopted our workflow for building an ISC model from our previous work,<sup>45</sup> but instead applied it to melt systems. The workflow is summarized in Figure 1. We first use an ESC model in different architectures, defined by  $N_{bb}$ ,  $N_{sc}$ , and  $f$ , that captures all of the side-chain degrees of freedom. SCMF simulation<sup>39</sup> is used to efficiently model bottlebrush polymers with this ESC representation in the melt state. This is a significant departure from our prior model, which used particle-based models that are computationally unable to model dense melts of long bottlebrush polymers. Next, the resulting conformations at equilibrium were analyzed by two observable quantities – end–end distance  $\langle R_{bb}^2 \rangle$  and radius of gyration  $\langle R_g^2 \rangle$  – to show that bottlebrush polymers can be modeled as a WLCy with the characteristic parameters of  $\lambda^{-1}$ ,  $L$ , and  $D$  that inform an ISC model. Finally, we used an iterative Boltzmann inversion (IBI) approach<sup>76</sup> to determine an effective pairwise potential so that the structure of this ISC model reproduces the structure of the ESC model. This is again a significant departure from our prior efforts, which used theoretically or simulation-determined pairwise potentials of mean force. IBI has the advantage that it also accounts for the higher-order correlations between dense bottlebrush chains.

## 2. BOTTLEBRUSH MODEL AND SIMULATION METHODS

Our workflow in Figure 1 consists of two types of simulations: (1) SCMF simulations of bottlebrush melts in the ESC representation, which are used to obtain conformational information for the WLCy model, and (2) BD simulations of bottlebrush polymers in the ISC representation, which, upon determination of an effective pair potential from the IBI procedure, are used to model melts at large length scales. In this section, we describe each of these simulation methods in detail.

**2.1. Single-Chain in Mean Field (SCMF) Simulation of the ESC Model.** The ESC model of bottlebrush polymers has  $N_{bb}$  backbone coarse-grained beads and  $N_{sc}$  side-chain beads, where  $f$  side chains are grafted per backbone bead. To study this model, we use the SCMF formalism, which is a field-based method that is discussed in detail in the literature;<sup>39,77</sup> we consider straightforward modifications of this method and only provide a brief outline of our approach. Our implementation of this approach considers coarse-grained beads on polymers  $i$  at monomer positions  $s$  at locations  $r_i(s)$ . Chains are modeled as Gaussian chains connected by a harmonic

bonding potential, and nonbonded interactions are included as a function of local densities  $\phi_A(\mathbf{r})$  and  $\phi_B(\mathbf{r})$  at spatial positions  $\mathbf{r}$ ,<sup>39</sup> where incompatible pair interactions are controlled by Flory–Huggins parameter  $\chi$  and compressibility parameter  $\kappa$ .<sup>39</sup> The total Hamiltonian  $\mathcal{H}$  is

$$\begin{aligned} \frac{\mathcal{H}[\{r_i(s)\}]}{k_B T} = & \frac{3}{2} \sum_{i=1}^n \sum_{s=1}^{N_{bb}'} \frac{(N_{bb}' - 1)[r_i(s+1) - r_i(s)]^2}{R_e'^2} \\ & + \rho_0 R_e'^3 / N \int_V \frac{d\mathbf{r}}{R_e'^3} \left[ \chi N \phi_A(\mathbf{r}) \phi_B(\mathbf{r}) + \frac{\kappa N}{2} (1 - \phi_A(\mathbf{r}) - \phi_B(\mathbf{r}))^2 \right] \end{aligned} \quad (1)$$

Here,  $b$  is a bond length,  $R_e'$  is a reference length scale associated with a reference chain backbone length  $N_{bb}'$ , via the relationship  $R_e'^2 = b^2(N_{bb}' - 1)\kappa$ .  $N$  represents the total number of beads used in a single bottlebrush chain (including both the backbone and side chain), and  $\rho_0$  is the system monomer density. In this paper, we only consider a homopolymer melt system, and thus the choice of  $\chi$  is zero while  $\kappa$  was chosen to be a sufficiently large value of 1.5625 so that  $\kappa N = 50$ .<sup>39</sup> The polymer density fields  $\phi_A(\mathbf{r})$  and  $\phi_B(\mathbf{r})$  are obtained from the bead positions in the discretized space following a “particle-to-mesh (PM)” method (Figure 2a).<sup>39</sup> This discretization consists of the  $n_{\text{sites}}$  number of grid points separated by a distance  $\Delta L$ , which

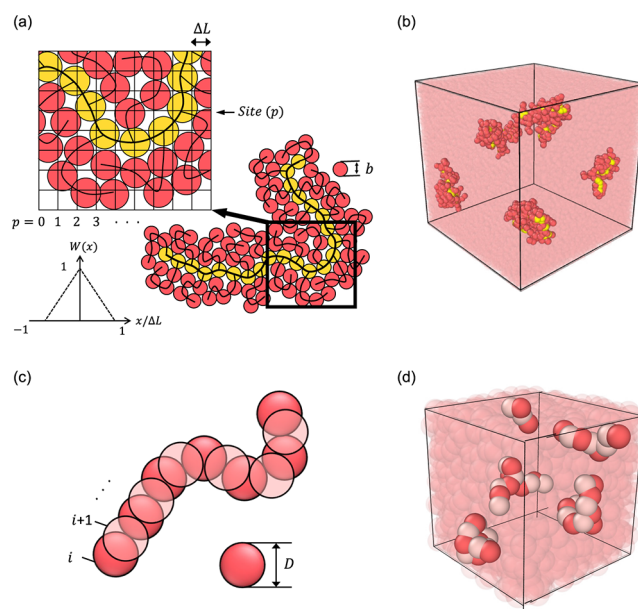


**Figure 2.** (a) Schematics of the PM method of SCMF simulation for an ESC model. Yellow spheres represent backbone beads, pink spheres represent side-chain beads, and black lines are simplified trajectories of beads. Positions of the beads are discretized by  $\Delta L$ , and local density at site  $p$ ,  $\phi(p)$ , is calculated by eq 2, which calculates normalized number density of neighboring ESC beads around site  $p$  given by the weight function  $W(x)$  as shown in the lower left. (b) Five representative ESC chains are illustrated in the simulation box of the bottlebrush melt system in the ESC model. All other ESC beads are set to be transparent. Periodic boundary is set to all box directions. (c) Schematic of an ISC chain for BD simulation. Each chain consists of total  $N_{\text{ISC}} = (2L - D)/D$  beads connected by bond length  $D/2$ , while each bead has diameter  $D$ . Bending potential is applied to three connected beads in the schematic with the bending constant  $\kappa_\theta = \lambda^{-1} k_B T / D$ . (d) Five representative ISC chains are illustrated in the simulation box of the bottlebrush melt system in the ISC mode. All other ISC beads are set to be transparent. Periodic boundary is set to all box directions.

determines the microscopic cutoff of the interaction range. The local density at the position  $\mathbf{r}$  is stored in a neighboring grid point  $p$  by

$$\phi(p) = 1/\rho^{\text{nor}} \sum_i W(\mathbf{r}_i - \mathbf{r}(p)) \quad (2)$$

where  $\rho^{\text{nor}}$  is the ideal average density at grid point  $p$  and  $W(\mathbf{r})$  represents the density weight at a grid point located a distance  $\mathbf{r}$  from a bead.<sup>39</sup> For simplicity,  $W(\mathbf{r})$  follows a first-order scheme<sup>39</sup> (see Figure 2a).

Traditional implementations of the SCMF method characterize the system with the chain length scale  $R_e$  and invariant degree of polymerization  $\sqrt{N} = \rho_0 R_e^3/N$ ; however, we want bottlebrush polymers with different  $N_{\text{bb}}$  and  $N_{\text{sc}}$  to all be modeled with consistent levels of coarse-graining.<sup>39,77</sup> We thus fix the length scale as  $b$ ,  $\Delta L$  as  $\Delta L = 0.65b$ , and run all simulations with respect to a constant reference backbone length  $N_{\text{bb}}' = 20$  with the corresponding reference distance  $R_e'$ . Upon choosing a length scale  $b = 0.74$  nm and molar mass per bead 200 g/mol (representing roughly two monomers), we can calculate a bead density  $\rho_0 = 1.207b^{-3}$  that is consistent with a real density of approximately 1 g/mL.<sup>78</sup> We can then determine the invariant degree of polymerization  $\sqrt{N}$  by either calculating  $R_e = b\sqrt{N_{\text{bb}}} - 1$  (Figure S1) or determining  $R_e$  from simulation (Figure S2). This quantity will provide insight into whether a given chain architecture and length is in the mean-field limit (which occurs for  $\sqrt{N} \rightarrow \infty$ ).<sup>39,48</sup> We plot the values of  $\sqrt{N}$  corresponding to various architectural features (i.e.,  $N_{\text{bb}}$ ,  $N_{\text{sc}}$ , and  $f$ ) in the Supporting Information (Figures S1 and S2). Both values of  $R_e$  that we consider show quantitative differences, but similar trends; simulation-based  $R_e$  values tend to be much larger due to branch-driven backbone stiffening, but even in this case  $\sqrt{N} \sim O(1 - 10)$ , indicating that we are far from the mean-field limit.

Configurations of the ESC bulk model are sampled using MC, and the energy difference between trial position and current position,  $\Delta E$ , used for the Metropolis criterion is based on the Hamiltonian consisting of bonded and nonbonded interactions as shown in eq 9. To efficiently find equilibrium configurations, in the first  $10^5$  time steps, the bond interaction is first equilibrated by only considering the harmonic bond term in  $\Delta E$ , after which the remaining contribution is included in  $\Delta E$  for the rest of the runtime. The total runtime is  $5 \times 10^6$  steps to sample the equilibrium conformations, and data was collected by averaging the samples over the final  $10^3$  steps. To avoid artificial oscillations in the density distribution,<sup>39</sup> the local densities are obtained by randomly shifting the grid.

## 2.2. Brownian Dynamics (BD) Simulation of the ISC Model.

BD simulations of the ISC model are used for bottlebrush homopolymer melts. The ISC beads follow a potential given by

$$U_{\text{total}} = U_b + U_\theta + U_{\text{nb}} \quad (3)$$

Here,  $U_b$  is a bond potential,  $U_\theta$  is a bending potential, and  $U_{\text{nb}}$  is a nonbonded potential. The bond potential used in our ISC model of bottlebrush homopolymer melts is in the form of a rigid Hookean spring between connected beads on  $n$  chains, chosen to maintain the contour length of the bottlebrush in the ISC model. In our previous work, we considered a tangent bead model with  $L/D$  beads kept at a distance  $D$  where they are immediately adjacent.<sup>44,45,54,70</sup> However, for our melt model, we find that this does not adequately reproduce a wormlike cylinder shape, and the accessible volume between beads negatively affects our IBI scheme. Instead, we consider  $N_{\text{ISC}} = (2L - D)/D$  beads that include both the set of tangent beads of diameter  $D$ , as well as intermediate beads connected at a distance  $D/2$  (see schematic in Figure 2c,d). The bond energy is thus:

$$U_b = \frac{\kappa_s}{2} \sum_j \sum_i^{N_{\text{ISC}}-1} \left( |\mathbf{r}_{i,j} - \mathbf{r}_{i+1,j}| - \frac{D}{2} \right)^2 \quad (4)$$

Here,  $\mathbf{r}_{i,j}$  is the position of bead  $i$  on chain  $j$ , and  $\kappa_s = 200k_B T/D^2$  is set to a relatively large value so that the bond is stiff and maintains a

nearly constant distance  $D/2$  between connected beads. Similarly, the bending potential for three connected beads on  $n$  chains is given as

$$U_\theta = \frac{\kappa_\theta}{2} \sum_j \sum_i^{N_{\text{ISC}}-2} (1 - \cos(\theta_{i,i+1,i+2})) \quad (5)$$

which reflects the stiffness of the ISC chain with the bending constant  $\kappa_\theta = \lambda^{-1}k_B T/D$  that includes Kuhn length  $\lambda^{-1}$ .<sup>44,54</sup> The bond angle for three connected beads with the distance  $D/2$  along the backbone is

$$\theta_{i,i+1,i+2} = \cos^{-1} \left( \frac{(\mathbf{r}_{i,j} - \mathbf{r}_{i+1,j}) \cdot (\mathbf{r}_{i+1,j} - \mathbf{r}_{i+2,j})}{|\mathbf{r}_{i,j} - \mathbf{r}_{i+1,j}| |\mathbf{r}_{i+1,j} - \mathbf{r}_{i+2,j}|} \right).$$

The nonbonded interaction is determined by an effective pairwise potential whose form will be described in Section 4. The total pairwise nonbonded interaction between any two beads  $i$  and  $j$  is the sum of all pairwise interactions.

$$U_{\text{nb}} = \sum_{k,l} \sum_{i>j}^{N_{\text{ISC}}} u_p(|\mathbf{r}_{i,k} - \mathbf{r}_{j,l}|) \quad (6)$$

The length units for  $D$  and  $\mathbf{r}$  are given as the bond length of the ESC bead  $b$ . We use a standard BD scheme that evolves the position of total  $N_{\text{tot}}$  ISC beads based on the assigned potentials via the Langevin equation:

$$\mathbf{R}(t + \delta t) = \mathbf{R}(t) - \nabla U(t) \delta t + \sqrt{2} \delta t \boldsymbol{\alpha} \quad (7)$$

where  $\mathbf{R}$  is the column vector of  $3N_{\text{tot}}$  positions,  $U(t)$  is total interaction potential described as  $U_{\text{total}} \delta t$  is the time step, and  $\boldsymbol{\alpha}$  is a column vector of length  $3N_{\text{tot}}$  containing random numbers from a normal distribution and reflects the displacement due to Brownian motion. The time step is normalized by the ISC bead diffusion time  $\tau = \zeta(b/2)^2/k_B T$ , where  $\zeta = 6\pi\eta_s b/2$  is the bead friction coefficient in a medium of viscosity  $\eta_s$ . The BD simulation is run for  $>10^5 \tau$  for equilibration, and data is collected from the final  $10^3$  time steps.

## 3. PARAMETERIZATION OF IMPLICIT SIDE-CHAIN (ISC) MODEL

We simulated both comb to bottlebrush polymers using the ESC model, considering parameters spanning a large range of backbone lengths  $N_{\text{bb}} = 10-110$ , side-chain lengths  $N_{\text{sc}} = 2, 4, 8, 14, 20$ , and grafting densities  $f = 1, 2, 5$ . We first analyzed the crowding parameter  $\Phi$  defined by Dobrynin et al.,<sup>33,46</sup> to classify the architecture space based on the extent of the overlap between neighboring brushes.<sup>33,46</sup> This parameter is calculated by a ratio of the volume occupied by monomers of a test macromolecule to its pervaded volume, and branched polymers can be distinguished as being in either comb ( $\Phi < 1$ ) or bottlebrush ( $\Phi > 1$ ) regimes.<sup>33</sup> We found that the crowding parameter  $\Phi$  ranges from 0.32 to 10.29 in our architecture space (Tables 1–3); strictly taking  $\Phi = 1$  as the criterion for

**Table 1. Fit Parameters at  $f = 1$**

$N_{\text{sc}}$	$m_L$	$\lambda^{-1}$ [b]	$D$ [b]	$L$ ( $N_{\text{bb}} = 100$ ) [b]	$\Phi = V/V_m$
2	0.73	3.33	4.5	72.27	0.32
4	0.62	5.26	5.9	61.38	0.51
8	0.54	8.00	8.2	53.46	0.92
14	0.49	13.33	10.8	48.51	1.55
20	0.49	18.18	12.9	48.51	2.31

distinguishing these two regimes, the samples at  $N_{\text{sc}} = 2, 4, 8$  at  $f = 1$  and  $N_{\text{sc}} = 2, 4$  at  $f = 2$  reside in comb regime while other architectures are all within the bottlebrush regime. We summarize these results using a diagram of the regimes in Figure S3. Notably, a higher  $\sqrt{N}$  is found for architectures with a lower crowding parameter (Figures S1 and S2). This is expected as the comb regime systems allow neighboring

**Table 2. Fit Parameters at  $f = 2$** 

$N_{sc}$	$m_L$	$\lambda^{-1}$ [b]	$D$ [b]	$L$ ( $N_{bb} = 100$ ) [b]	$\Phi = V/V_m$
2	0.68	5.00	5.0	66.84	0.54
4	0.61	8.33	6.5	60.39	0.94
8	0.60	12.50	8.8	59.40	1.81
14	0.60	17.51	11.8	59.40	3.12
20	0.60	26.32	13.8	59.40	4.37

**Table 3. Fit Parameters at  $f = 5$** 

$N_{sc}$	$m_L$	$\lambda^{-1}$ [b]	$D$ [b]	$L$ ( $N_{bb} = 100$ ) [b]	$\Phi = V/V_m$
2	1.20	4.76	5.4	118.8	1.17
4	1.20	7.14	7.2	118.8	2.16
8	1.20	10.53	10.0	118.8	4.23
14	1.20	16.67	13.0	118.8	7.31
20	1.20	22.22	15.6	118.8	10.29

macromolecules to interpenetrate due to a weak crowding effect,<sup>33,79</sup> implying that individual chains do not as strongly exclude other chains compared to systems with a high crowding parameter. However, we note that the criteria of comb and bottlebrushes are not a strict boundary and expect situations where  $\Phi \approx 1$  to represent intermediate cases.<sup>33,46</sup>

We used the SCMF simulations to obtain the end–end distance  $\langle R_{bb}^2 \rangle$  of the backbone and the radius of gyration  $\langle R_g^2 \rangle$ . The values for  $\langle R_{bb}^2 \rangle$  and  $\langle R_g^2 \rangle$  are plotted as a function of  $N_{bb}$  in Figures 3 and 4, respectively, for several side-chain lengths  $N_{sc}$  and grafting densities  $f$ . The conformations of bottlebrushes in the melt are much less extended ( $\langle R_{bb}^2 \rangle \sim 10^3 b^2$  for  $N_{bb} = 100$ ,  $N_{sc} = 20$  and  $f = 5$  for example) than their counterparts in dilute solution (with  $\langle R_{bb}^2 \rangle \sim 10^4 b^2$ ),<sup>45</sup> due to the enhanced flexibility of the chains in the absence of solvent and thus strong excluded volume repulsions between side chains.<sup>33,45,46,71–74</sup> This is evident in the scaling exponents  $2\nu \approx 1$  in both  $\langle R_{bb}^2 \rangle$  and  $\langle R_g^2 \rangle$  at higher  $N_{bb}$ , demonstrating that the chains exhibit limiting behavior consistent with a Gaussian coil conformation.<sup>45,80</sup> This is a consequence of our new coarse-graining scheme, which explicitly uses molecular models suitable for polymer melts. However, our SCMF model prediction shows a general trend where longer and more densely grafted side chains induce more stretched conformations along the backbone, leading to increased chain

dimensions with increasing  $N_{sc}$ .<sup>33,46,65</sup> At low values of  $N_{bb}$ , this effect on  $\langle R_{bb}^2 \rangle$  becomes relatively small, not stretching the backbone much for all  $f$  due to the star-like conformation.<sup>45,81</sup> Conversely, for  $\langle R_g^2 \rangle$  (Figure 4), this results in a plateau in  $\langle R_g^2 \rangle$  as the side-chain length becomes the major contributor of the conformation, again due to the star-like architecture.<sup>45,65,81</sup> This upturn is less apparent at higher grafting density (i.e.,  $f = 5$ , Figure 4c), which is capable of stretching even for relatively short backbone contours.

Following protocols for ISC parametrization established in our previous work, we fit the simulation data using expressions for a Kratky–Porod (KP) chain<sup>82,83</sup> and WLCy model, which are indicated as dashed lines in Figures 3 and 4.<sup>45</sup> The end–end distance of the unperturbed KP chain is given by<sup>82</sup>

$$\langle R_{bb}^2 \rangle_0 = \frac{L}{\lambda} - \frac{1}{2\lambda^2}(1 - e^{-2\lambda L}) \quad (8)$$

The radius of gyration of WLCy chain is given by<sup>83</sup>

$$\langle R_g^2 \rangle_0 = \frac{L}{6\lambda} - \frac{1}{4\lambda^2} + \frac{1}{4\lambda^3 L} - \frac{1}{8\lambda^4 L^2}(1 - e^{-2\lambda L}) + \frac{D^2}{8} \quad (9)$$

In both these expressions,  $L$  is the cylinder length,  $\lambda^{-1}$  is effective Kuhn length of the bottlebrush, and  $D$  is the width of the cylinder. Unlike the dilute solution situation, we did not consider the  $B$  parameter due to the screening of excluded volume interactions in a melt system.<sup>45</sup> Therefore, we can adopt these unperturbed expressions of eqs 8 and 9 to fit the conformation of the ESC bottlebrush in the melt. In the fitting of  $\langle R_{bb}^2 \rangle$ , a constant of proportionality  $m_L = L(N_{bb} - 1)$  was used instead of  $L$  as the fitting parameter along with  $\lambda^{-1}$ , such that each set of parameters corresponds to the entire series of data at various  $N_{bb}$  for a given  $f$  and  $N_{sc}$ . Then, as the parameters  $m_L$  and  $\lambda^{-1}$  are obtained from the  $\langle R_{bb}^2 \rangle$  fitting,  $D$  remained the only parameter to fit  $\langle R_g^2 \rangle$ . Importantly,  $D$  is obtained by fitting results in the low- $N_{bb}$  limit, where  $D$  plays a dominant role on bottlebrush dimensions.<sup>45,65,81</sup> The fit results are denoted as dashed lines in Figures 3 and 4, and the corresponding parameters are tabulated in Tables 1–23 and plotted in Figure 5 in comparison with our prior results for dilute solution.<sup>45</sup>

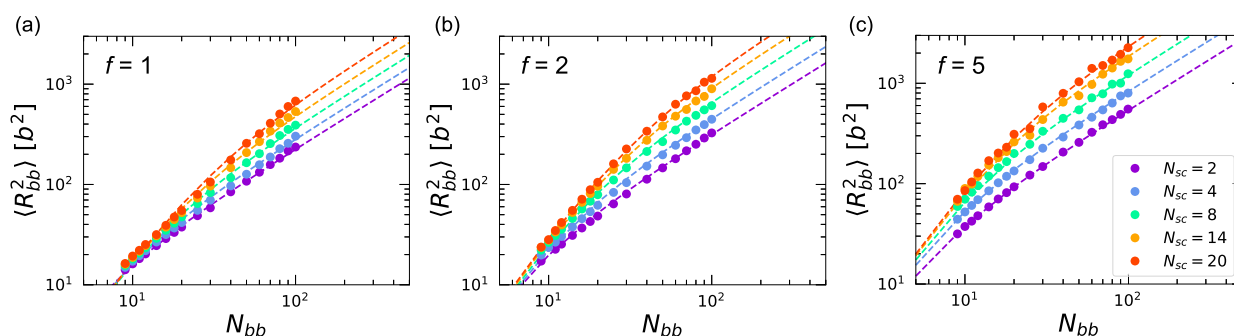


**Figure 3.** End-to-end distance  $\langle R_{bb}^2 \rangle$  versus bottlebrush backbone length  $N_{bb}$  at (a)  $f = 1$ , (b)  $f = 2$  and (c)  $f = 5$  for several side-chain lengths  $N_{sc}$ . Markers denote the SCMF data, and dashed lines denote the fitting data using the unperturbed KP expression for in eq 8, assuming a constant proportionality between the contour length and backbone degree of polymerization,  $L = m_L(N_{bb} - 1)$ , for each value of  $N_{sc}$ . Fit parameters  $m_L$  and  $\lambda^{-1}$  are summarized in Tables 1–3. For all cases, the end-to-end distance increases with increasing side-chain length; however, this effect is small for short backbone lengths  $N_{bb}$  due to star-like conformations.<sup>45,81</sup>

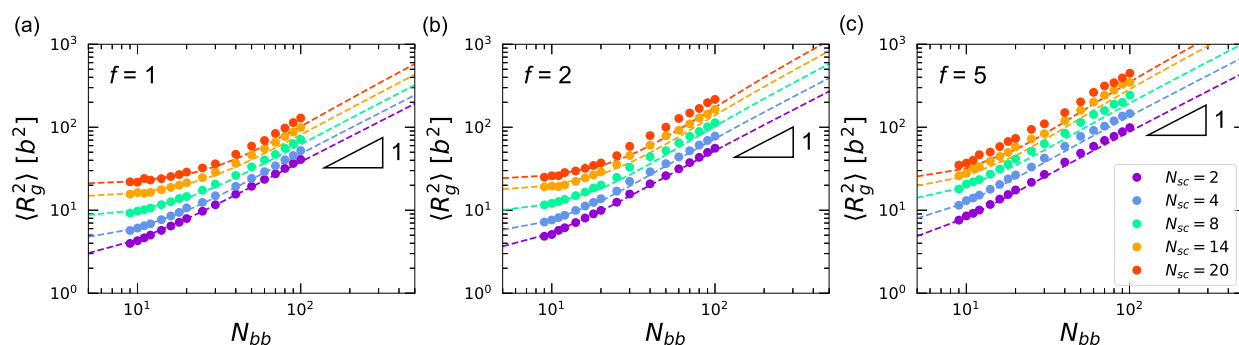


**Figure 4.** Radius of gyration  $\langle R_g^2 \rangle$  versus bottlebrush backbone length  $N_{bb}$  at (a)  $f = 1$ , (b)  $f = 2$  and (c)  $f = 5$  for several side-chain lengths  $N_{sc}$ . Markers denote the SCMF data, and dashed lines denote the fitting data using unperturbed WLCy expression for  $\langle R_g^2 \rangle$  in eq 9, using the values of  $m_L$  and  $\lambda^{-1}$  determined from the  $\langle R_{bb}^2 \rangle$  data in Figure 3. The remaining fit parameter is the bottlebrush width  $D$ , which is summarized in Tables 1–3. For all cases, the radius of gyration increases when the side chains get longer and more densely grafted, and this effect is largest for short backbone lengths  $N_{bb}$  because  $N_{sc}$  is the major contributor to the size  $\langle R_g^2 \rangle$  in the star-like conformations.

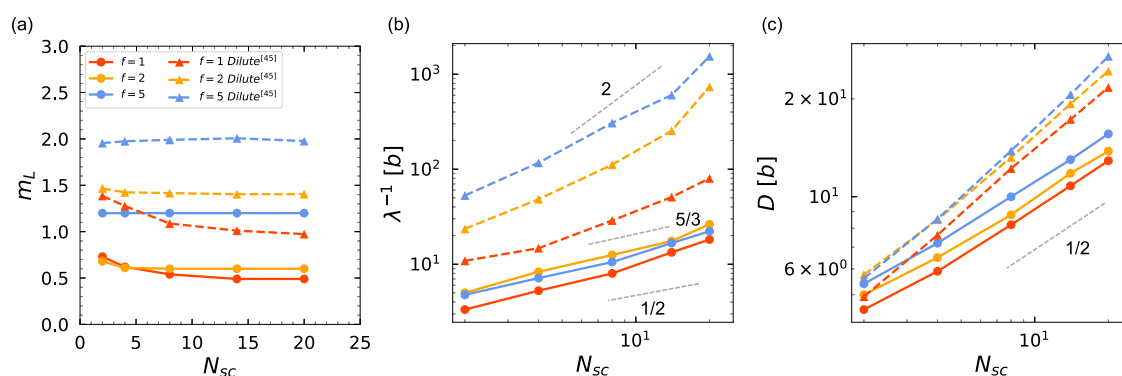


**Figure 5.** Comparison of fit parameters to analogous dilute solution parameters from our prior work.<sup>45</sup> Circle markers connected by solid lines represent the fit parameters for melts, while triangle markers connected by dashed lines represent the fit parameters from dilute solution. (a) The proportionality between the contour length and backbone degree of polymerization,  $m_L$ , is highly reduced in melts when compared with dilute solution quantities, while also showing increasingly stretched conformations with increasing grafting density. (b) The Kuhn length  $\lambda^{-1}$  is smaller in melts than dilute solution, which scaling exponent is  $\approx 1/2$  that is consistent with predictions by Rubinstein and Dobrynin.<sup>33,46</sup> Dashed gray lines denote the relevant scaling exponents. (c) The bottlebrush width  $D$  is smaller in melts than in dilute solution and exhibits a scaling exponent of  $1/2$  following Gaussian chain statistics.<sup>33,46,84</sup> The data from dilute solution are adapted with permission from ref.<sup>45</sup> Copyright 2019 American Chemical Society.

The curves of  $\langle R_{bb}^2 \rangle$  and  $\langle R_g^2 \rangle$  versus  $N_{bb}$  fit well to the unperturbed expressions of  $\langle R_{bb}^2 \rangle$  and  $\langle R_g^2 \rangle$  with a single set of fitting parameters  $m_L$ ,  $\lambda^{-1}$ , and  $D$ . We confirmed that there is good agreement between the geometric value  $D$  and the side chain radius of gyration  $\langle R_{g,sc}^2 \rangle^{1/2}$  (Table S1), and all increase by  $N_{sc}$  with the scaling exponent of  $1/2$  as reported by Rubinstein and Dobrynin.<sup>33,46</sup> However, we observed slight deviations in  $\langle R_g^2 \rangle$  at high  $N_{bb}$ , which we attribute to the neglect of quantitative perturbations from short-ranged interactions in the fit curve (eq 9) that is related to the local packing correlations of the thick bottlebrush chains in the melt state.<sup>82,83</sup> This is also apparent when we look at the ratio of  $\langle R_{bb}^2 \rangle / \langle R_g^2 \rangle$ , which is meaningfully reduced from the factor of 6 expected for an ideal chain (Table S1).<sup>84</sup> Nevertheless, representing the melt bottlebrush conformation as an “effective” ideal chain is still possible, as the perturbation due to the nonlinear architecture does not affect the scaling exponent associated with the Gaussian chain conformation.<sup>33,46</sup> The set of parameters can now be used as the parameters for an ISC model that can be used for large-scale

simulations, with the primary approximation being that the number of ISC beads  $N_{ISC}$  in a chain is set to  $N_{ISC} = (2L - D)/D$ , which is the nearest integer number  $L/D$  with the intermediate beads to maintain the WLCy shape. Example ISC model fit parameters for  $N_{bb} = 100$  are shown in Table S2.

The approach taken in this paper represents a unique opportunity to compare and contrast the melt versus dilute solution conformations of bottlebrush polymers in the context of related molecular models. Our fit parameters demonstrate that melt bottlebrushes are highly flexible, such that the Kuhn length  $\lambda^{-1}$  spans from  $\sim 10^0 b$  to  $\sim 10^1 b$  (i.e., within several backbone monomers) compared to the dilute case where  $\lambda^{-1}$  spans from  $\sim 10^1 b$  to  $\sim 10^4 b$  in a similar architectural space,<sup>45</sup> which we attribute to the screening of excluded volume interactions in the melt state.<sup>33,46,65,72</sup> (Figure 5b). We note that the length units of the ESC model for polymer melts are not quite the same as in the corresponding model for dilute solutions, with the former being chosen as  $b = 0.74$  for melts and  $b = 0.67$  for solutions. This difference is quantitatively modest, but we also note that these represent different physical models as well, with the SCMF representation assuming a Gaussian monomer, while the (semi)dilute model uses hard

particles. This will prevent a quantitative comparison at monomer-level length scales, but we are focusing on larger chain length scales and assume that the two models are different by a proportionality factor of order unity.

Significant differences between the solution and melt bottlebrush conformations are also apparent when comparing the scaling relationships observed and/or predicted in the literature.<sup>33,46,79,85–87</sup> For dilute solution, the bottlebrush Kuhn length is expected to increase by  $\lambda^{-1} \sim N_{sc}^2$  for sufficiently high grafting density<sup>85,86</sup> or  $\lambda^{-1} \sim N_{sc}^{3/5} \sim D$  when approaching the self-avoiding walk limit,<sup>79</sup> while Rubinstein and Dobrynin predicted  $\lambda^{-1} \sim D \sim N_{sc}^{1/2}$  for a bottlebrush melt.<sup>33,46</sup> We found that the scaling exponent does indeed exhibit a scaling of  $\lambda^{-1} \sim D \sim N_{sc}^{1/2}$ <sup>33,46</sup> consistent with the scaling argument as shown in Figure 5b,c that the side chains exhibit Gaussian conformations. The stiffening of the bottlebrush polymer is thus present even in the absence of the excluded volume interactions that drive the large Kuhn length in dilute solutions.<sup>33,46</sup> While we have studied only a few select grafting densities  $f$  that limits the conclusions we can draw about the relationship between  $\lambda^{-1}$  and  $f$ ,  $\lambda^{-1}$  appears to be similar between  $f = 5$  versus  $f = 2$ , but both are indeed stiffer than the lower-branch density  $f = 1$  case. More dramatic trends are observed with respect to  $N_{sc}$ , manifesting as a linear relationship between the crowding parameter  $\Phi$  and the stiffness  $\lambda^{-1}$  at fixed  $f$  that is consistent with the scaling theory for bottlebrush melts.<sup>33,46</sup> Even though  $\lambda^{-1}$  can be approximated with  $D$ ,<sup>33,46,79</sup> it appears to be slightly quantitatively smaller than  $D$  ( $\lambda^{-1} \lesssim D$ ) at smaller  $N_{sc}$  and  $f$ , but is slightly larger than  $D$  ( $\lambda^{-1} \gtrsim D$ ) for larger  $N_{sc}$  and  $f$ . This transition happens at a crowding parameter  $\Phi \approx 1$ , which is where the backbone stretching becomes dominant, leading to a stiff conformation.

The backbone is also affected by architectural parameters and in particular is sensitive to the grafting density as shown in Figure 5a. For  $f = 1$  and 2, the proportionality factor  $m_L < 1$  indicates that the backbone is less stretched than expected for the equivalent wormlike cylinder around a linear chain. This shrinkage becomes more pronounced as  $N_{sc}$  is increased. This is consistent with our previous work<sup>45,55</sup> and is attributed to the extended random walk of the backbone within the overall chain contour. This effect becomes sufficiently weak at large  $N_{sc}$  that the fit is not sensitive to  $m_L$ , which remains unchanged over several values of  $N_{sc}$  in our fitting procedure. However, there is a more noticeable effect of  $f$ , such that chains are slightly more stretched for  $f = 2$  versus  $f = 1$ , and  $f = 5$  shows significantly more stretching with  $m_L > 1$ . This is a characteristic attribute of bottlebrush melts that the enhanced backbone flexibility competes with a stiffening effect due to increased grafting density.<sup>72</sup> This behavior has ramifications for our coarse-graining scheme, because  $L$  and  $D$  do not follow the same trend with respect to grafting density  $f$ ; the nearest integer of  $L/D$  exhibits a weaker increase with grafting density compared to the dilute solution situation.<sup>45</sup>

#### 4. PAIRWISE INTERACTION POTENTIAL OF ISC MODEL

Fitting the ESC model to the WLCy model allows us to predict single-chain conformational properties but does not account for the pairwise interaction potential needed to capture the structure of the bottlebrush polymers in the melt state. To our

knowledge, there is no analytical model for the pairwise interaction potential of these ISC beads, due to the challenge of accounting for the correlation hole of extended side chains.<sup>22,46,64,75</sup> Therefore, we decided to use IBI to determine the effective pair potential  $u_p(r)$  between ISC beads.<sup>76</sup> The IBI method improves on a “guess” potential  $u_{p,n}(r)$  in each iteration  $n$  by using the differences between the pair distribution function  $g_n(r)$  from this potential and the true “target” pair distribution function  $g_{target}(r)$  from a fine-grained or atomistic model to determine a new potential  $u_{p,n+1}(r)$ .<sup>76</sup> While this method only accounts for the radial pair correlations  $g(r)$  between segments, it is known to accurately reproduce the actual configurations of molecules in various polymer melt systems.<sup>76,88–90</sup> We adopted this method for our system and summarized the detailed implementation as a flowchart in Figure 6.

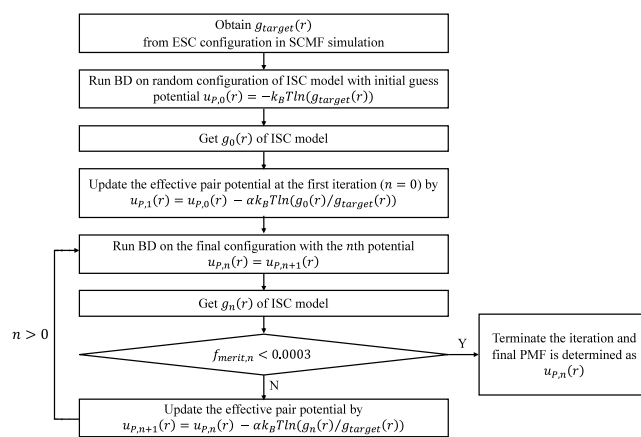


**Figure 6.** Flowchart of IBI implementation for finding the effective pairwise potential  $u_p(r)$  for ISC model.  $g_{target}(r)$  is calculated directly by coarse-graining the ESC chain configurations based on the discretization scheme for the ISC model. BD simulations of the ISC model are performed using an initial guess potential  $u_{p,0}(r)$  that is obtained from the direct Boltzmann inverse of  $g_{target}(r)$ . The difference between the resulting equilibrium correlations  $g_0(r)$  and target correlations  $g_{target}(r)$  is used to modify the potential from  $u_{p,0}(r) \rightarrow u_{p,1}(r)$ , which is then used in a subsequent  $n = 1$  iteration to calculate an updated  $g_1(r)$ . Each iteration loop thus consists of BD simulations using the  $n$ th potential  $u_{p,n}(r)$  to calculate  $g_n(r)$ ; the difference between  $g_n(r)$  and  $g_{target}(r)$  is used to calculate a new potential  $u_{p,n+1}(r)$  and merit function  $f_{merit}^n$  (eq 12) that indicates convergence when  $f_{merit}^n < 3 \times 10^{-4}$ .

We start by calculating the target  $g_{target}(r)$  directly from the initial ESC chain configurations, based on a discretization scheme that defines an “effective” ISC bead by dividing the ESC backbone into  $N_{ISC}$  portions. The center of mass of each of these backbone segments and corresponding side chains is chosen as the coordinate for the effective ISC model and contributes to the overall target  $g_{target}(r)$ . We consider all pairs except the adjacent pairs in a chain (e.g.,  $i$ th and  $i + 1$ th beads in Figure 2c) that are not physically interacting with the same pair potential.

Representative final target  $g_{target}(r)$  functions for several different architectures with  $N_{bb} = 100$  are presented in Figure 7, with distances in units of the  $b$ , the bond distance of the ESC bead. As expected, all  $g_{target}(r)$  curves exhibit a significant depletion at small  $r$  (i.e.,  $g_{target}(r) < 1$ ), which is consistent with a segmental correlation hole. This is an important feature of

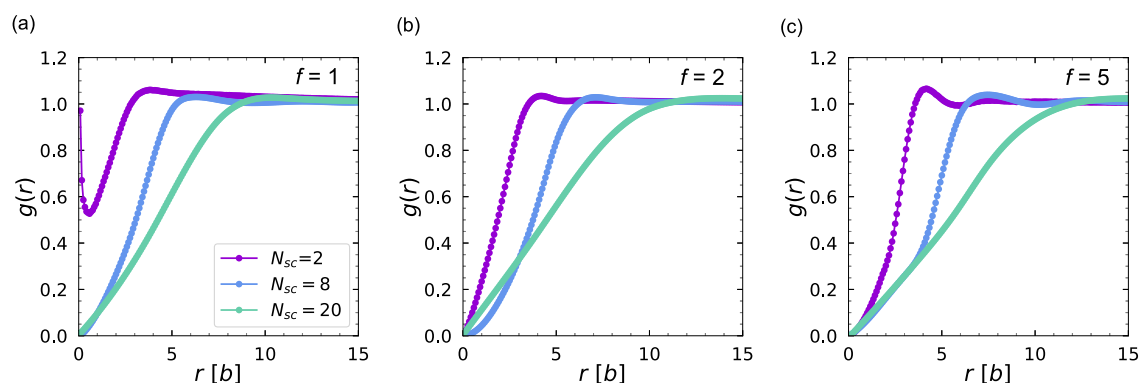


**Figure 7.** Target distribution function  $g_{\text{target}}(r)$  at (a)  $f = 1$ , (b)  $f = 2$ , and (c)  $f = 5$  for different side chain lengths  $N_{\text{sc}} = 2, 8, 20$  and  $N_{\text{bb}} = 100$ , generated by averaging the final 100 MC steps of an SCMF simulation. All curves exhibit a significant depletion at small  $r$  (i.e.,  $g_{\text{target}}(r) < 1$ ) as neighboring bottlebrush polymers do not fully overlap due to a high local density of side chains near the backbone. This effect is less prominent in the comblike limit of  $f = 1$  and  $N_{\text{sc}} = 2$ . This correlation hole grows as the side-chain length  $N_{\text{sc}}$  gets longer and correspondingly the bottlebrush width  $D$  gets larger. The emergence of a small overshoot in  $g_{\text{target}}(r)$  at  $r \sim D$  is observed as  $f$  is increased, indicating packing of adjacent bottlebrushes as the conformation approaches the hard cylinder limit.

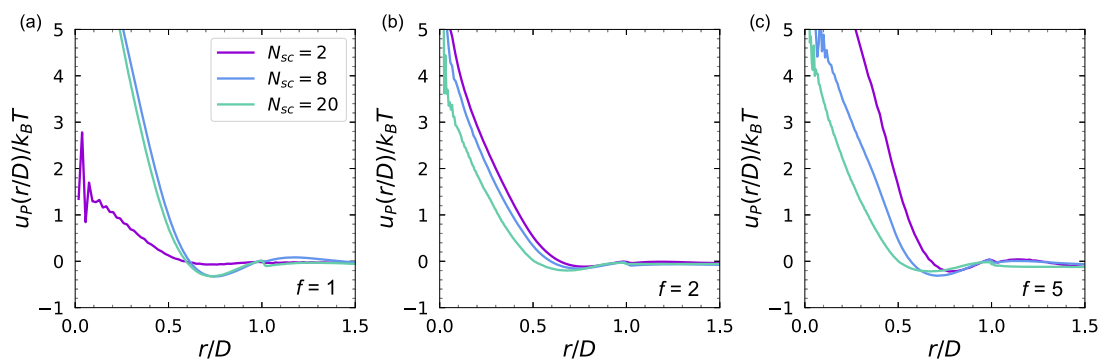


**Figure 8.** Optimized pair potential  $u_p(r)$  of ISC model, determined by the IBI procedure outlined in Figure 6 at (a)  $f = 1$ , (b)  $f = 2$  and (c)  $f = 5$  for several different side-chain lengths  $N_{\text{sc}} = 2, 8$ , and  $20$ . Relative to the bottlebrush width  $D$ , the soft pairwise repulsion between bottlebrush chain segments generally appears shorter-ranged as the side-chain length  $N_{\text{sc}}$  increases due to the decreased radial packing of side chains from the backbone for a given grafting density  $f$ . The primary exception to this is in (a) for the comb architecture  $f = 1$  and  $N_{\text{sc}} = 2$ , which exhibits a particularly weak repulsion ( $u_p(r \rightarrow 0) \approx 1.5k_B T$ ) that corresponds to the shallow correlation hole seen in Figure 7a. All bottlebrush architectures also have an attractive portion around  $0.5\text{--}0.7r/D$ , which arises due to the packing of molecules as also shown in Figure 7.

our use of the SCMF model; it indicates that neighboring bottlebrush polymers do not fully overlap, due to the exclusion imposed by the finite concentration of the side chains. A significant amount of side-chain driven exclusion is consistent with the conceptual scaling picture described by Dobrynin et al. and indeed becomes notably less pronounced in the comblike limit of  $f = 1$  and  $N_{\text{sc}} = 2$  (Figure 7a) where  $\Phi \ll 1$ .<sup>33,46,64</sup> This correlation hole grows as the side-chain length  $N_{\text{sc}}$  gets longer and correspondingly the bottlebrush width  $D$  gets larger. The role of  $f$  is more subtle as demonstrated in Figure S4, which plots  $g_{\text{target}}(r)$  for different values of  $f$  at each  $N_{\text{sc}}$ . These are the same plots of  $g_{\text{target}}(r)$  in Figure 7a–c, but they are plotted to show the modest increase in the range of  $r$  over which depletion occurs with  $f$ . This is consistent with the behavior of  $D$ , which similarly changes only weakly with  $f$  as seen in Tables 1–23. The other notable feature of these pair correlation functions is the emergence of a small overshoot in  $g_{\text{target}}(r)$  at  $r \sim D$  as  $f$  is increased. This is especially prominent in Figure 7c for  $f = 5$  and  $N_{\text{sc}} = 2$ , where the bottlebrush most approaches a hard flexible “cylinder”, where there is a defined distance  $\approx D$  of packing and liquid-like correlations between adjacent molecules.

Our IBI scheme seeks to determine  $u_p(r)$  based on BD simulations of randomly placed ISC chains, with the goal of

reproducing  $g_{\text{target}}(r)$  for the same density as the ESC model. We used the bond and bending potentials discussed in Section 2.2, with the bending constant  $\kappa_\theta$  based on the tabulated  $\lambda^{-1}$  for the ISC model in Tables 1–3. The initial guess for the pairwise potential  $u_{p,0}(r)$  was chosen as the Boltzmann inversion of  $g_{\text{target}}(r)$ :

$$u_{p,0}(r) = -k_B T \ln(g_{\text{target}}(r)) \quad (10)$$

This expression is only exact in the limit of highly dilute systems, but it is sufficient to provide an initial guess to be modified by IBI.<sup>76,88,91</sup> For each iteration  $n$ , the initial structure is determined from an  $n$ th guess potential  $u_{p,n}$  via a BD simulation run for  $>10^5 \tau$  timesteps. The  $g_n(r)$  is collected for the final 1000  $\tau$  and compared with  $g_{\text{target}}(r)$  to determine a new guess for the pairwise potential  $u_{p,n+1}$  that will be used for the  $n + 1$  iteration:

$$u_{p,n+1}(r) = u_{p,n}(r) - \alpha k_B T \ln \left( \frac{g_n(r)}{g_{\text{target}}(r)} \right) \quad (11)$$

Here,  $\alpha$  is a scaling coefficient that is set to 0.005 to maintain stability.<sup>88</sup> This iterative scheme is carried out until there is a

convergence of  $g_n(r)$  to  $g_{\text{target}}(r)$ , as evaluated by a merit function for each iteration  $n$ ,  $f_{\text{merit},n}$ :

$$f_{\text{merit},n} = \frac{\int [g_n(r) - g_{\text{target}}(r)]^2 dr}{\int [g_{\text{target}}(r)]^2 dr} \quad (12)$$

when  $f_{\text{merit},n} < 3 \times 10^{-4}$ , the system is determined to be converged.<sup>88</sup> Figure S5 shows how  $g_n(r)$  evolves during iteration to the final  $g_{\text{target}}(r)$ .

We plot the potentials  $u_p(r)$  obtained from IBI for different architectures in Figure 8, as a function of  $r/D$  to normalize against the underlying bottlebrush width, as determined by our coarse-graining scheme. The features of the  $u_p(r)$  curves are consistent over almost all architectures considered and in particular exhibit a similar repulsive contribution for short distances  $r$ . This feature is notably soft for most of the architectures, when compared against conventional potential forms like Lennard-Jones (LJ) or Weeks–Chandler–Andersen (WCA), and for larger bottlebrushes ( $N_{\text{sc}} > 2$  and  $f > 1$ ), the value of the pair potential only reaches  $u_p(r) \sim 5k_{\text{B}}T$  even at  $r \sim 0$ . Relative to bottlebrush width  $D$ , this repulsion appears shorter-ranged as the side-chain length  $N_{\text{sc}}$  increases. This can be attributed to the decreased radial packing of side chains further away from the backbone for a given grafting density  $f$ , which leads to weaker repulsion at the side-chain ends for larger  $N_{\text{sc}}$ , as long as the chain is sufficiently in the bottlebrush regime. The notable exception to this trend is  $u_p(r)$  for  $N_{\text{sc}} = 2$  and  $f = 1$  (Figure 8a), which is in the comb regime and thus exhibits a particularly weak repulsion ( $u_p(r \rightarrow 0) \approx 1.5k_{\text{B}}T$ ) that corresponds to the shallow correlation hole in Figure 7a.

We also compared the effective pair potential  $u_p(r)$  at different grafting densities  $f$  for several side-chain lengths  $N_{\text{sc}}$  in Figure S6, replotting the data in Figure 8 to facilitate comparison. At  $N_{\text{sc}} = 2$ , the pair potential exhibits a stronger repulsion as grafting density increases, which we attribute to the increased packing of side chains in going from the weak comb-regime potential at  $f = 1$  to the bottlebrush regime at  $f = 5$ . However, this trend no longer holds for longer side chains,  $N_{\text{sc}} = 8, 20$ . For both of these cases,  $u_p(r)$  shows the strongest repulsion at  $f = 1$ . However, this is not a large effect; the  $u_p(r)$  curves for  $f = 2$  and  $f = 5$  are only modestly weaker than that for  $f = 1$  and have similar strengths to each other. The general expectation that higher values of  $f$  lead to stronger repulsions is complicated by our normalization of  $r$  by  $D$ , which increases meaningfully with  $f$ . These effects appear to roughly cancel out, leading to a remarkably consistent pair potential  $u_p(r/D)$  for all bottlebrushes in the high  $N_{\text{sc}}$  and  $f$  limits. While this does not appear to represent a true “collapse” to a universal form of the pair potential, at least near the parameters considered here, it may be possible to estimate  $u_p(r/D)$  for other architectures.

The other feature that is common to almost all bottlebrush architectures is an attractive portion of  $u_p(r/D)$  around  $r/D \approx 0.5$ – $0.7$ . This portion is related to the overshoot in the  $g_{\text{target}}(r)$  discussed previously, and we attribute to the correlated packing of bottlebrush molecules in the equilibrium, melt state.<sup>84,92</sup> Similar features have been predicted or observed previously in both bottlebrush melts<sup>46,93–95</sup> and polyelectrolyte solutions.<sup>96–99</sup> A small feature in  $u_p(r)$  at  $r/D \approx 1$  is observed in all pair potentials and is due to the correlation between beads connected at the distance  $r \approx D$  via a hard spring potential in the ISC model. The resulting strong correlations do not appear in the ESC model (i.e.,  $g_{\text{target}}(r)$ ), because the SCMF

simulation does not enforce a specific distance between coarse-grained beads. This feature is visually apparent, but its magnitude is significantly smaller than  $k_{\text{B}}T$  so we do not expect it to be physically meaningful. Modest fluctuations above the distance  $r/D = 1$  are also seen, but the IBI procedure is known to have low accuracy for long-ranged interactions and is not expected to make a major contribution to the properties of polymer melts<sup>84,92</sup> or chain conformations.

## 5. DISCUSSION AND CONCLUSION

We proposed a scheme to determine a coarse-grained model of bottlebrush polymers in melts, using an ISC representation that was previously successful in understanding bottlebrush polymers in solution.<sup>44,45,54,70</sup> This coarse-grained representation was built on an ESC model for melt bottlebrush polymers that used PM-SCMF simulations. This importantly allowed us to consider nonmean-field structures, which are crucial to accounting for the significant correlation holes expected in a bottlebrush polymer (and implied by scaling approaches e.g., by Dobrynin et al.<sup>33,46</sup>). Our system was set to a range of values of  $\sqrt{N}$ , which was chosen to be low enough to span the comb-to-bottlebrush transition and roughly correspond to the overlap parameter  $\Phi$ . This condition allowed us to characterize the architecture-driven conformations of homopolymer bottlebrush melts, including correlations that would otherwise be smeared out in mean-field approximations. Previous efforts using the SCMF model for bottlebrush polymers focused on conditions close to the mean-field limit,<sup>49,100</sup> which do not recapitulate the side-chain driven exclusion of neighboring bottlebrushes from the near-backbone regions.

The geometric components of this ISC model, namely, the length scales, number of the coarse-grained beads  $N_{\text{ISC}}$ , and their bending potentials  $\kappa_{\theta}$ , were determined directly from the ESC model. Chain dimensions from SCMF simulations,  $\langle R_{\text{bb}}^2 \rangle$  and  $\langle R_{\text{g}}^2 \rangle$ , were used to fit the theoretical expressions of KP chain and WLCy model, simplifying entire sets of bottlebrush architectures at a variety of backbone lengths  $N_{\text{bb}}$  (but at given  $N_{\text{sc}}$  and  $f$ ) to a single set of fit parameters for the wormlike cylinder model ( $m_{\text{L}}$ ,  $\lambda^{-1}$ ,  $D$ ). We confirmed that the conformation of bottlebrush polymers in melt exhibits random walk scaling  $\nu = 1/2$  at sufficiently long values of  $N_{\text{bb}}$  but with varying widths  $D$  and Kuhn length  $\lambda^{-1}$ . The fit parameters showed that the limiting conformations of bottlebrush polymers in the melt state are less stiff and stretched compared to the dilute solution due to the high concentration of polymers and screening of solvent-mediated excluded volume interactions. However, we still found that backbone stretching does occur, especially when there is a high density of grafted side chains ( $f = 5$ ), and the Kuhn length  $\lambda^{-1}$  does increase with  $\Phi$  as predicted by the prior literature.<sup>33,46</sup> Both properties are correlated with localized crowding and steric constraints of the side chains along the backbone.

Finally, bottlebrush–bottlebrush interactions were incorporated into the ISC model framework using the IBI method. The  $g_{\text{target}}(r)$  exhibits structural features characteristic of bottlebrush polymers, in particular, soft interactions that nevertheless exhibit significant steric exclusion of neighboring chains near the bottlebrush backbone. The goal of this ISC model is to expedite molecular models of bottlebrush structure and assembly, similar to how the solution ISC model has allowed for molecular predictions consistent with both dynamic properties and self-assembled structure observed in

experiments.<sup>44,67,70</sup> These types of coarse-grained models will be especially important in making predictions for bottlebrush assembly in the melt state. While there has been some success in using field theoretic<sup>14,16,101–103</sup> or SCMF methods<sup>48,100</sup> to account for these types of systems, further coarse-graining such as in this ISC framework will facilitate the modeling of large-scale assembly of self-assembled bottlebrush polymers in a way that (1) allows for the consideration of truly large bottlebrush polymers, such as those commonly synthesized in experiments that have  $O(10^3)$  backbone monomers,<sup>104–106</sup> and (2) the consideration of bottlebrush polymers with nonstandard architectures,<sup>34,47,107,108</sup> including variations of side chains along the contour (i.e., shape-defined bottlebrush polymers)<sup>47,52,107,108</sup> and variations in grafting density.<sup>58,108,109</sup> Future efforts to model similar systems will require modifications to this method, however, to account for multiple components with the effect of  $\chi$ , and the variation of the coarse-grained ISC parameters along the backbone.

## ■ ASSOCIATED CONTENT

### SI Supporting Information

The Supporting Information is available free of charge at <https://pubs.acs.org/doi/10.1021/acs.macromol.4c01038>.

Details about the methods for the bottlebrush polymers; ratio of end–end distance and radius of gyration and radius of gyration of side chains (Table S1); ISC model parameters (Table S2); calculation of  $\sqrt{N}$  (Figures S1 and S2); diagram of the regimes by architecture  $N_{sc}$  and  $f$  based on crowding parameter  $\Phi$  (Figure S3); target distribution function  $g_{\text{target}}(r)$  (Figure S4); convergence of  $g(r)$  in IBI procedure (Figure S5); optimized effective pair potential of ISC model by the convergence of IBI procedure (Figure S6) (PDF)

## ■ AUTHOR INFORMATION

### Corresponding Author

Charles E. Sing – Department of Chemical and Biomolecular Engineering, University of Illinois Urbana–Champaign, Urbana, Illinois 61801, United States; [orcid.org/0000-0001-7231-2685](https://orcid.org/0000-0001-7231-2685); Email: [cesing@illinois.edu](mailto:cesing@illinois.edu)

### Authors

Haisu Kang – Department of Chemical and Biomolecular Engineering, University of Illinois Urbana–Champaign, Urbana, Illinois 61801, United States

Tianyuan Pan – Department of Chemical and Biomolecular Engineering, University of Illinois Urbana–Champaign, Urbana, Illinois 61801, United States; [orcid.org/0000-0002-8837-1230](https://orcid.org/0000-0002-8837-1230)

Complete contact information is available at:

<https://pubs.acs.org/doi/10.1021/acs.macromol.4c01038>

### Funding

This work was supported by the National Science Foundation under the Designing Materials to Revolutionize and Engineer our Future (DMREF) award number DMR-2119172 and the American Chemical Society (ACS) Petroleum Research Fund under award Number 61500-ND7.

### Notes

The authors declare no competing financial interest.

## ■ REFERENCES

- (1) Xie, G.; Martinez, M. R.; Olszewski, M.; Sheiko, S. S.; Matyjaszewski, K. Molecular Bottlebrushes as Novel Materials. *Biomacromolecules* **2019**, *20* (1), 27–54.
- (2) Pan, T.; Dutta, S.; Kamble, Y.; Patel, B. B.; Wade, M. A.; Rogers, S. A.; Diao, Y.; Guirounet, D.; Sing, C. E. Materials Design of Highly Branched Bottlebrush Polymers at the Intersection of Modeling, Synthesis, Processing, and Characterization. *Chem. Mater.* **2022**, *34* (5), 1990–2024.
- (3) Nam, J.; Kim, Y.; Kim, J. G.; Seo, M. Self-Assembly of Monolayer Vesicles via Backbone-Shiftable Synthesis of Janus Core–Shell Bottlebrush Polymer. *Macromolecules* **2019**, *52* (24), 9484–9494.
- (4) Fang, A.; Lin, S.; Ng, F. T. T.; Pan, Q. Synthesis of Core-Shell Bottlebrush Polymers of Poly(Polycaprolactone-*b*-Polyethylene Glycol) via Ring-Opening Metathesis Polymerization. *J. Macromol. Sci., Part A* **2022**, *59* (1), 20–30.
- (5) Varlas, S.; Hua, Z.; Jones, J. R.; Thomas, M.; Foster, J. C.; O'Reilly, R. K. Complementary Nucleobase Interactions Drive the Hierarchical Self-Assembly of Core–Shell Bottlebrush Block Copolymers toward Cylindrical Supramolecules. *Macromolecules* **2020**, *53* (22), 9747–9757.
- (6) Nese, A.; Li, Y.; Averick, S.; Kwak, Y.; Konkolewicz, D.; Sheiko, S. S.; Matyjaszewski, K. Synthesis of Amphiphilic Poly(N-Vinylpyrrolidone)-*b*-Poly(Vinyl Acetate) Molecular Bottlebrushes. *ACS Macro Lett.* **2012**, *1* (1), 227–231.
- (7) Yamauchi, Y.; Yamada, K.; Ishida, Y. Synthesis of Water-Soluble Bottlebrush Polymer with Hydrophobic Core and Hydrophilic Shell as Cylindrical Host for Guest Uptake. *Chem. Lett.* **2019**, *48* (11), 1410–1413.
- (8) Li, Z.; Tang, M.; Liang, S.; Zhang, M.; Biesold, G. M.; He, Y.; Hao, S.-M.; Choi, W.; Liu, Y.; Peng, J.; Lin, Z. Bottlebrush Polymers: From Controlled Synthesis, Self-Assembly, Properties to Applications. *Prog. Polym. Sci.* **2021**, *116*, 101387.
- (9) Verduzco, R.; Li, X.; Pesek, S. L.; Stein, G. E. Structure, Function, Self-Assembly, and Applications of Bottlebrush Copolymers. *Chem. Soc. Rev.* **2015**, *44* (8), 2405–2420.
- (10) Cui, S.; Zhang, B.; Shen, L.; Bates, F. S.; Lodge, T. P. Core–Shell Gyroid in ABC Bottlebrush Block Terpolymers. *J. Am. Chem. Soc.* **2022**, *144* (47), 21719–21727.
- (11) Song, Q.; Dong, Q.; Liang, R.; Xue, Y.; Zhong, M.; Li, W. Hierarchical Self-Assembly of ABC-Type Bottlebrush Copolymers. *Macromolecules* **2023**, *56* (14), 5470–5481.
- (12) Chen, K.; Hu, X.; Zhu, N.; Guo, K. Design, Synthesis, and Self-Assembly of Janus Bottlebrush Polymers. *Macromol. Rapid Commun.* **2020**, *41* (20), 2000357.
- (13) Karavolias, M. G.; Elder, J. B.; Ness, E. M.; Mahanthappa, M. K. Order-to-Disorder Transitions in Lamellar Melt Self-Assembled Core–Shell Bottlebrush Polymers. *ACS Macro Lett.* **2019**, *8* (12), 1617–1622.
- (14) Chen, D.; Quah, T.; Delaney, K. T.; Fredrickson, G. H. Investigation of the Self-Assembly Behavior of Statistical Bottlebrush Copolymers via Self-Consistent Field Theory Simulations. *Macromolecules* **2022**, *55* (20), 9324–9333.
- (15) Yang, Y.; Lin, S.; Feng, X.; Pan, Q. Synthesis and Characterization of Core-Shell Bottlebrush Polymers via Controllable Polymerization. *ChemistrySelect* **2022**, *7* (25), No. e202201040.
- (16) Liu, R.; Sun, Z.; Huang, H.; Johnson, J. A.; Alexander-Katz, A.; Ross, C. A. Experimental and Computational Evaluation of Self-Assembled Morphologies in Diblock Janus Bottlebrush Copolymers. *Nano Lett.* **2023**, *23* (1), 177–182.
- (17) Liberman-Martin, A. L.; Chang, A. B.; Chu, C. K.; Siddique, R. H.; Lee, B.; Grubbs, R. H. Processing Effects on the Self-Assembly of Brush Block Polymer Photonic Crystals. *ACS Macro Lett.* **2021**, *10* (12), 1480–1486.
- (18) Wang, Z.; Chan, C. L. C.; Zhao, T. H.; Parker, R. M.; Vignolini, S. Recent Advances in Block Copolymer Self-Assembly for the Fabrication of Photonic Films and Pigments. *Adv. Opt. Mater.* **2021**, *9* (21), 2100519.

- (19) Seong, H.-G.; Fink, Z.; Chen, Z.; Emrick, T.; Russell, T. P. Bottlebrush Polymers at Liquid Interfaces: Assembly Dynamics, Mechanical Properties, and All-Liquid Printed Constructs. *ACS Nano* **2023**, *17* (15), 14731–14741.
- (20) Yi, H.; Li, Y.; Song, D. Hierarchical Assemblies of Bottlebrush/Homopolymer Blends: Tailoring Phase Interfacial Curvature for Tunable Photonics †. *Chin. J. Chem.* **2023**, *41* (13), 1566–1574.
- (21) Xu, H.; Sun, F. C.; Shirvanyants, D. G.; Rubinstein, M.; Shabratov, D.; Beers, K. L.; Matyjaszewski, K.; Sheiko, S. S. Molecular Pressure Sensors. *Adv. Mater.* **2007**, *19* (19), 2930–2934.
- (22) Reynolds, V. G.; Mukherjee, S.; Xie, R.; Levi, A. E.; Atassi, A.; Uchiyama, T.; Wang, H.; Chabiny, M. L.; Bates, C. M. Super-Soft Solvent-Free Bottlebrush Elastomers for Touch Sensing. *Mater. Horiz.* **2020**, *7* (1), 181–187.
- (23) Xiong, H.; Zhang, L.; Wu, Q.; Zhang, H.; Peng, Y.; Zhao, L.; Huang, G.; Wu, J. A. Strain-Adaptive, Self-Healing, Breathable and Perceptive Bottle-Brush Material Inspired by Skin. *J. Mater. Chem. A* **2020**, *8* (46), 24645–24654.
- (24) Lee, H.; Boyce, J. R.; Nese, A.; Sheiko, S. S.; Matyjaszewski, K. pH-Induced Conformational Changes of Loosely Grafted Molecular Brushes Containing Poly(Acrylic Acid) Side Chains. *Polymer* **2008**, *49* (25), 5490–5496.
- (25) Kim, H.; Watkins, J. J.; Crosby, A. J. Adhesion and Mechanical Properties of Poly (Dimethylsiloxane) Bottlebrush Elastomers. *Soft Matter* **2023**, *19* (28), 5311–5317.
- (26) Laws, T. S.; Mei, H.; Terlier, T.; Verduzco, R.; Stein, G. E. Tailoring the Wettability and Substrate Adherence of Thin Polymer Films with Surface-Segregating Bottlebrush Copolymer Additives. *Langmuir* **2023**, *39* (20), 7201–7211.
- (27) Milatz, R.; Duvigneau, J.; Vancso, G. J. Dopamine-Based Copolymer Bottlebrushes for Functional Adhesives: Synthesis, Characterization, and Applications in Surface Engineering of Antifouling Polyethylene. *ACS Appl. Mater. Interfaces* **2023**, *15* (28), 34023–34030.
- (28) Self, J. L.; Sample, C. S.; Levi, A. E.; Li, K.; Xie, R.; De Alaniz, J. R.; Bates, C. M. Dynamic Bottlebrush Polymer Networks: Self-Healing in Super-Soft Materials. *J. Am. Chem. Soc.* **2020**, *142* (16), 7567–7573.
- (29) Xie, R.; Lapkriengkri, I.; Pramanik, N. B.; Mukherjee, S.; Blankenship, J. R.; Albanese, K.; Wang, H.; Chabiny, M. L.; Bates, C. M. Hydrogen-Bonding Bottlebrush Networks: Self-Healing Materials from Super-Soft to Stiff. *Macromolecules* **2022**, *55* (23), 10513–10521.
- (30) Choi, C.; Self, J. L.; Okayama, Y.; Levi, A. E.; Gerst, M.; Speros, J. C.; Hawker, C. J.; Read De Alaniz, J.; Bates, C. M. Light-Mediated Synthesis and Reprocessing of Dynamic Bottlebrush Elastomers under Ambient Conditions. *J. Am. Chem. Soc.* **2021**, *143* (26), 9866–9871.
- (31) Keith, A. N.; Clair, C.; Lallam, A.; Bersenev, E. A.; Ivanov, D. A.; Tian, Y.; Dobrynin, A. V.; Sheiko, S. S. Independently Tuning Elastomer Softness and Firmness by Incorporating Side Chain Mixtures into Bottlebrush Network Strands. *Macromolecules* **2020**, *53* (21), 9306–9312.
- (32) Xu, P.; Wang, S.; Lin, A.; Min, H.-K.; Zhou, Z.; Dou, W.; Sun, Y.; Huang, X.; Tran, H.; Liu, X. Conductive and Elastic Bottlebrush Elastomers for Ultrasoft Electronics. *Nat. Commun.* **2023**, *14* (1), 623.
- (33) Liang, H.; Cao, Z.; Wang, Z.; Sheiko, S. S.; Dobrynin, A. V. Combs and Bottlebrushes in a Melt. *Macromolecules* **2017**, *50* (8), 3430–3437.
- (34) Sheiko, S. S.; Sumerlin, B. S.; Matyjaszewski, K. Cylindrical Molecular Brushes: Synthesis, Characterization, and Properties. *Prog. Polym. Sci.* **2008**, *33* (7), 759–785.
- (35) Namba, S.; Tsukahara, Y.; Kaeriyama, K.; Okamoto, K.; Takahashi, M. Bulk Properties of Multibranching Polystyrenes from Polystyrene Macromonomers: Rheological Behavior I. *Polymer* **2000**, *41* (14), 5165–5171.
- (36) Tsukahara, Y.; Ohta, Y.; Senoo, K. Liquid Crystal Formation of Multibranching Polystyrene Induced by Molecular Anisotropy Associated with Its High Branch Density. *Polymer* **1995**, *36* (17), 3413–3416.
- (37) Wintermantel, M.; Fischer, K.; Gerle, M.; Ries, R.; Schmidt, M.; Kajiwar, K.; Urakawa, H.; Wataoka, I. Lyotropic Phases Formed by “Molecular Bottlebrushes”. *Angew. Chem., Int. Ed.* **1995**, *34* (13–14), 1472–1474.
- (38) Hsu, H.-P.; Paul, W.; Binder, K. Polymer Chain Stiffness vs. Excluded Volume: A Monte Carlo Study of the Crossover towards the Worm-like Chain Model. *Europhys. Lett.* **2010**, *92* (2), 28003.
- (39) Detcheverry, F. A.; Kang, H.; Daoulas, K. C.; Müller, M.; Nealey, P. F.; De Pablo, J. J. Monte Carlo Simulations of a Coarse Grain Model for Block Copolymers and Nanocomposites. *Macromolecules* **2008**, *41* (13), 4989–5001.
- (40) Fytas, N. G.; Theodorakis, P. E. Molecular Dynamics Simulations of Single-Component Bottle-Brush Polymers with Flexible Backbones under Poor Solvent Conditions. *J. Phys.: Condens. Matter* **2013**, *25* (28), 285105.
- (41) Chen, G.; Dormidontova, E. Atomistic Molecular Dynamics Simulations of Cyclic Bottlebrush Polymers. *Macromolecules* **2023**, *56* (9), 3286–3295.
- (42) Lyubimov, I.; Wessels, M. G.; Jayaraman, A. Molecular Dynamics Simulation and PRISM Theory Study of Assembly in Solutions of Amphiphilic Bottlebrush Block Copolymers. *Macromolecules* **2018**, *51* (19), 7586–7599.
- (43) Dutta, S.; Sing, C. E. Brownian Dynamics Simulations of Bottlebrush Polymers in Dilute Solution under Simple Shear and Uniaxial Extensional Flows. *J. Chem. Phys.* **2024**, *160* (4), 044901.
- (44) Pan, T.; Patel, B. B.; Walsh, D. J.; Dutta, S.; Guironnet, D.; Diao, Y.; Sing, C. E. Implicit Side-Chain Model and Experimental Characterization of Bottlebrush Block Copolymer Solution Assembly. *Macromolecules* **2021**, *54* (8), 3620–3633.
- (45) Dutta, S.; Pan, T.; Sing, C. E. Bridging Simulation Length Scales of Bottlebrush Polymers Using a Wormlike Cylinder Model. *Macromolecules* **2019**, *52* (13), 4858–4874.
- (46) Paturej, J.; Sheiko, S. S.; Panyukov, S.; Rubinstein, M. Molecular Structure of Bottlebrush Polymers in Melts. *Sci. Adv.* **2016**, *2* (11), No. e1601478.
- (47) Walsh, D. J.; Dutta, S.; Sing, C. E.; Guironnet, D. Engineering of Molecular Geometry in Bottlebrush Polymers. *Macromolecules* **2019**, *52* (13), 4847–4857.
- (48) Park, S. J.; Kim, J. U. Single Chain in Mean Field Simulation of Flexible and Semiflexible Polymers: Comparison with Discrete Chain Self-Consistent Field Theory. *Soft Matter* **2020**, *16* (22), 5233–5249.
- (49) Park, J.; Thapar, V.; Choe, Y.; Padilla Salas, L. A.; Ramírez-Hernández, A.; de Pablo, J. J.; Hur, S.-M. Coarse-Grained Simulation of Bottlebrush: From Single-Chain Properties to Self-Assembly. *ACS Macro Lett.* **2022**, *11* (9), 1167–1173.
- (50) Hsu, H.-P.; Paul, W.; Binder, K. Structure of bottle-brush polymers in solution: A Monte Carlo test of models for the scattering function. *J. Chem. Phys.* **2008**, *129*, 204904.
- (51) Kang, J.-J.; Sachse, C.; Ko, C.-H.; Schroer, M. A.; Vela, S. D.; Molodenskiy, D.; Kohlbrecher, J.; Bushuev, N. V.; Gumerov, R. A.; Potemkin, I. I.; Jordan, R.; Papadakis, C. M. Rigid-to-Flexible Transition in a Molecular Brush in a Good Solvent at a Semidilute Concentration. *Langmuir* **2022**, *38* (17), 5226–5236.
- (52) Alaboalir, M.; Scannelli, S. J.; Rahmaninejad, H.; Carrillo, J.-M.; Do, C.; Matson, J. B.; Ashkar, R. Solution Structure and Scaling Laws of Cylindrical and Tapered Bottlebrush Polymers. *Macromolecules* **2023**, *56* (22), 9264–9276.
- (53) Salinas-Soto, C. A.; Choe, Y.; Hur, S.-M.; Ramírez-Hernández, A. Exploring Conformations of Comb-like Polymers with Varying Grafting Density in Dilute Solutions. *J. Chem. Phys.* **2023**, *159* (11), 114901.
- (54) Pan, T.; Dutta, S.; Sing, C. E. Interaction Potentials for Coarse-Grained Models of Bottlebrush Polymers. *J. Chem. Phys.* **2022**, *156*, 014903.
- (55) Dutta, S.; Sing, C. E. Two Stretching Regimes in the Elasticity of Bottlebrush Polymers. *Macromolecules* **2020**, *53* (16), 6946–6955.
- (56) Dalsin, S. J.; Rions-Maehren, T. G.; Beam, M. D.; Bates, F. S.; Hillmyer, M. A.; Matsen, M. W. Bottlebrush Block Polymers:

- Quantitative Theory and Experiments. *ACS Nano* **2015**, *9* (12), 12245–12245.
- (57) Detcheverry, F. A.; Pike, D. Q.; Nagpal, U.; Nealey, P. F.; De Pablo, J. J. Theoretically Informed Coarse Grain Simulations of Block Copolymer Melts: Method and Applications. *Soft Matter* **2009**, *5* (24), 4858.
- (58) Lin, T.-P.; Chang, A. B.; Luo, S.-X. L.; Chen, H.-Y.; Lee, B.; Grubbs, R. H. Effects of Grafting Density on Block Polymer Self-Assembly: From Linear to Bottlebrush. *ACS Nano* **2017**, *11* (11), 11632–11641.
- (59) Zhulina, E. B.; Borisov, O. V. Micelles Formed by an AB Copolymer with Bottlebrush Blocks: Scaling Theory. *J. Phys. Chem. B* **2021**, *125* (45), 12603–12616.
- (60) Cao, Z.; Daniel, W. F. M.; Vatankhah-Varnosfaderani, M.; Sheiko, S. S.; Dobrynin, A. V. Dynamics of Bottlebrush Networks. *Macromolecules* **2016**, *49* (20), 8009–8017.
- (61) Mohammadi, E.; Joshi, S. Y.; Deshmukh, S. A. A Review of Computational Studies of Bottlebrush Polymers. *Comput. Mater. Sci.* **2021**, *199*, 110720.
- (62) Raj, W.; Halagan, K.; Kadubowski, S.; Maczugowska, P.; Szutkowski, K.; Jung, J.; Pietrasik, J.; Jurga, S.; Sikorski, A. The Structure and Dynamics of Bottlebrushes: Simulation and Experimental Studies Combined. *Polymer* **2022**, *261*, 125409.
- (63) Xiong, H.; Yue, T.; Wu, Q.; Zhang, L.; Xie, Z.; Liu, J.; Zhang, L.; Wu, J. Self-Healing Bottlebrush Polymer Networks Enabled via a Side-Chain Interlocking Design. *Mater. Horiz.* **2023**, *10* (6), 2128–2138.
- (64) Paturej, J.; Kreer, T. Hierarchical Excluded Volume Screening in Solutions of Bottlebrush Polymers. *Soft Matter* **2017**, *13* (45), 8534–8541.
- (65) Zhulina, E. B.; Sheiko, S. S.; Borisov, O. V. Solution and Melts of Barbwire Bottlebrushes: Hierarchical Structure and Scale-Dependent Elasticity. *Macromolecules* **2019**, *52* (4), 1671–1684.
- (66) Dutta, S.; Wade, M. A.; Walsh, D. J.; Guirionnet, D.; Rogers, S. A.; Sing, C. E. Dilute Solution Structure of Bottlebrush Polymers. *Soft Matter* **2019**, *15* (14), 2928–2941.
- (67) Jeon, S.; Kamble, Y. L.; Kang, H.; Shi, J.; Wade, M. A.; Patel, B. B.; Pan, T.; Rogers, S. A.; Sing, C. E.; Guirionnet, D.; Diao, Y. Direct-Ink-Write Cross-Linkable Bottlebrush Block Copolymers for on-the-Fly Control of Structural Color. *Proc. Natl. Acad. Sci. U. S. A.* **2024**, *121* (9), No. e2313617121.
- (68) Nakamura, Y.; Norisuye, T. *Brush-Like Polymers*; Springer: Dordrecht, Netherlands, 2008.
- (69) Wintermantel, M.; Schmidt, M.; Tsukahara, Y.; Kajiwara, K.; Kohjiya, S. Rodlike Combs. *Macromol. Rapid Commun.* **1994**, *15* (3), 279–284.
- (70) Patel, B. B.; Pan, T.; Chang, Y.; Walsh, D. J.; Kwok, J. J.; Park, K. S.; Patel, K.; Guirionnet, D.; Sing, C. E.; Diao, Y. Concentration-Driven Self-Assembly of PS-*b*-PLA Bottlebrush Diblock Copolymers in Solution. *ACS Polym. Au* **2022**, *2* (4), 232–244.
- (71) Nian, S.; Huang, B.; Freychet, G.; Zhernenkov, M.; Cai, L.-H. Unexpected Folding of Bottlebrush Polymers in Melts. *Macromolecules* **2023**, *56* (6), 2551–2559.
- (72) Daniel, W. F. M.; Burdyńska, J.; Vatankhah-Varnosfaderani, M.; Matyjaszewski, K.; Paturej, J.; Rubinstein, M.; Dobrynin, A. V.; Sheiko, S. S. Solvent-Free, Supersoft and Superelastic Bottlebrush Melts and Networks. *Nat. Mater.* **2016**, *15* (2), 183–189.
- (73) Chan, J. M.; Kordon, A. C.; Zhang, R.; Wang, M. Direct Visualization of Bottlebrush Polymer Conformations in the Solid State. *Proc. Natl. Acad. Sci. U. S. A.* **2021**, *118* (40), No. e2109534118.
- (74) Chan, J. M.; Kordon, A. C.; Wang, M. Investigating the Effects of the Local Environment on Bottlebrush Conformations Using Super-Resolution Microscopy. *Nanoscale* **2024**, *16* (5), 2409–2418.
- (75) Sunday, D. F.; Chremos, A.; Martin, T. B.; Chang, A. B.; Burns, A. B.; Grubbs, R. H. Concentration Dependence of the Size and Symmetry of a Bottlebrush Polymer in a Good Solvent. *Macromolecules* **2020**, *53* (16), 7132–7140.
- (76) Reith, D.; Pütz, M.; Müller-Plathe, F. Deriving Effective Mesoscale Potentials from Atomistic Simulations: Mesoscale Potentials from Atomistic Simulations. *J. Comput. Chem.* **2003**, *24* (13), 1624–1636.
- (77) Müller, M.; Smith, G. D. Phase Separation in Binary Mixtures Containing Polymers: A Quantitative Comparison of Single-Chain-in-Mean-Field Simulations and Computer Simulations of the Corresponding Multichain Systems. *J. Polym. Sci., Part B: Polym. Phys.* **2005**, *43* (8), 934–958.
- (78) Hiemenz, P. C.; Lodge, T. *Polymer Chemistry*, 2nd ed.; CRC Press: Boca Raton, FL, 2007.
- (79) Birshtein, T. M.; Borisov, O. V.; Zhulina, B. Y.; Khokhlov, A. R.; Yurasova, T. A. Conformations of Comb-like Macromolecules. *Polym. Sci. U.S.S.R.* **1987**, *29* (6), 1293–1300.
- (80) Yamakawa, H.; Yoshizaki, T. *Helical Wormlike Chains in Polymer Solutions*; Springer: Berlin, Heidelberg, 2016.
- (81) Zografos, A.; All, H. A.; Chang, A. B.; Hillmyer, M. A.; Bates, F. S. Star-to-Bottlebrush Transition in Extensional and Shear Deformation of Unentangled Polymer Melts. *Macromolecules* **2023**, *56* (6), 2406–2417.
- (82) Benoit, H.; Doty, P. Light Scattering from Non-Gaussian Chains. *J. Phys. Chem.* **1953**, *57* (9), 958–963.
- (83) Konishi, T.; Yoshizaki, T.; Saito, T.; Einaga, Y.; Yamakawa, H. Mean-Square Radius of Gyration of Oligo- and Polystyrenes in Dilute Solutions. *Macromolecules* **1990**, *23* (1), 290–297.
- (84) Rubinstein, M.; Colby, R. H. *Polymer Physics*; Oxford University Press: New York, 2003.
- (85) Fredrickson, G. H. Surfactant-Induced Lyotropic Behavior of Flexible Polymer Solutions. *Macromolecules* **1993**, *26* (11), 2825–2831.
- (86) Subbotin, A.; Saariaho, M.; Ikkala, O.; ten Brinke, G. Elasticity of Comb Copolymer Cylindrical Brushes. *Macromolecules* **2000**, *33* (9), 3447–3452.
- (87) Nakamura, Y.; Norisuye, T. Backbone Stiffness of Comb-Branched Polymers. *Polym. J.* **2001**, *33* (11), 874–878.
- (88) Agrawal, V.; Arya, G.; Oswald, J. Simultaneous Iterative Boltzmann Inversion for Coarse-Graining of Polyurea. *Macromolecules* **2014**, *47* (10), 3378–3389.
- (89) Johnson, L. C.; Phelan, F. R., Jr. Dynamically Consistent Coarse-Grain Simulation Model of Chemically Specific Polymer Melts via Friction Parameterization. *J. Chem. Phys.* **2021**, *154* (8), 084114.
- (90) Peters, B. L.; Salerno, K. M.; Agrawal, A.; Perahia, D.; Grest, G. S. Coarse-Grained Modeling of Polyethylene Melts: Effect on Dynamics. *J. Chem. Theory Comput.* **2017**, *13* (6), 2890–2896.
- (91) Zhu, Z.; Luo, X.; Paddison, S. J. Coarse-Grained Modeling of Ion-Containing Polymers. *Chem. Rev.* **2022**, *122* (12), 10710–10745.
- (92) Fredrickson, G. H. *The Equilibrium Theory of Inhomogeneous Polymers*; Oxford University Press: New York, 2006.
- (93) Clark, A. J.; McCarty, J.; Guenza, M. G. Effective Potentials for Representing Polymers in Melts as Chains of Interacting Soft Particles. *J. Chem. Phys.* **2013**, *139* (12), 124906.
- (94) Akkermans, R. L. C.; Briels, W. J. Coarse-Grained Interactions in Polymer Melts: A Variational Approach. *J. Chem. Phys.* **2001**, *115* (13), 6210–6219.
- (95) Chremos, A.; Nikoubashman, A.; Panagiotopoulos, A. Z. Flory-Huggins Parameter  $\chi$ , from Binary Mixtures of Lennard-Jones Particles to Block Copolymer Melts. *J. Chem. Phys.* **2014**, *140* (5), 054909.
- (96) da Silva, F. L. B.; Jönsson, B. Polyelectrolyte–Protein Complexation Driven by Charge Regulation. *Soft Matter* **2009**, *5* (15), 2862–2868.
- (97) Forsyth, M.; Payne, V. A.; Ratner, M. A.; de Leeuw, S. W.; Shriver, D. F. Molecular Dynamics Simulations of Highly Concentrated Salt Solutions: Structural and Transport Effects in Polymer Electrolytes. *Solid State Ion.* **1992**, *53–56*, 1011–1026.
- (98) Shen, K.-H.; Fan, M.; Hall, L. M. Molecular Dynamics Simulations of Ion-Containing Polymers Using Generic Coarse-Grained Models. *Macromolecules* **2021**, *54* (5), 2031–2052.

- (99) Shen, K.-H.; Hall, L. M. Ion Conductivity and Correlations in Model Salt-Doped Polymers: Effects of Interaction Strength and Concentration. *Macromolecules* **2020**, *53* (10), 3655–3668.
- (100) Niu, Y.; Bu, X.; Zhang, X. Single Chain Mean-Field Theory Study on Responsive Behavior of Semiflexible Polymer Brush. *Materials* **2021**, *14* (4), 778.
- (101) Vigil, D. L.; Quah, T.; Sun, D.; Delaney, K. T.; Fredrickson, G. H. Self-Consistent Field Theory Predicts Universal Phase Behavior for Linear, Comb, and Bottlebrush Diblock Copolymers. *Macromolecules* **2022**, *55* (11), 4237–4244.
- (102) Spencer, R. K. W.; Matsen, M. W. Field-Theoretic Simulations of Bottlebrush Copolymers. *J. Chem. Phys.* **2018**, *149* (18), 184901.
- (103) Park, S. J.; Cheong, G. K.; Bates, F. S.; Dorfman, K. D. Stability of the Double Gyroid Phase in Bottlebrush Diblock Copolymer Melts. *Macromolecules* **2021**, *54* (19), 9063–9070.
- (104) Dalsin, S. J.; Hillmyer, M. A.; Bates, F. S. Molecular Weight Dependence of Zero-Shear Viscosity in Atactic Polypropylene Bottlebrush Polymers. *ACS Macro Lett.* **2014**, *3* (5), 423–427.
- (105) Jha, S.; Dutta, S.; Bowden, N. B. Synthesis of Ultralarge Molecular Weight Bottlebrush Polymers Using Grubbs' Catalysts. *Macromolecules* **2004**, *37* (12), 4365–4374.
- (106) Seo, H.-B.; Yu, Y.-G.; Chae, C.-G.; Kim, M.-J.; Lee, J.-S. Synthesis of Ultrahigh Molecular Weight Bottlebrush Block Copolymers of  $\omega$ -End-Norbornyl Polystyrene and Polymethacrylate Macromonomers. *Polymer* **2019**, *177*, 241–249.
- (107) Kamble, Y. L.; Walsh, D. J.; Guironnet, D. Precision of Architecture-Controlled Bottlebrush Polymer Synthesis: A Monte Carlo Analysis. *Macromolecules* **2022**, *55* (23), 10255–10263.
- (108) Walsh, D. J.; Guironnet, D. Macromolecules with Programmable Shape, Size, and Chemistry. *Proc. Natl. Acad. Sci. U. S. A.* **2019**, *116* (5), 1538–1542.
- (109) Xiao, L.; Li, J.; Peng, G.; Huang, G. The Effect of Grafting Density and Side Chain Length on the Conformation of PEG Grafted Bottlebrush Polymers. *React. Funct. Polym.* **2020**, *156*, 104736.